Enhanced suppression of longitudinal vibration transmission in propulsion shaft system using a nonlinear inerter device

Wei Dai[a], Baiyang Shi[b], Jian Yang*[b], Xiang Zhu[a], Tianyun Li[a]

[a]*School of Naval Architecture and Ocean Engineering, Huazhong University of Science and Technology, Wuhan 430074, P.R. China.*

[b]*Faculty of Science and Engineering, University of Nottingham Ningbo China, Ningbo 315100, P.R. China.*

*Corresponding author: jian.yang@nottingham.edu.cn

Abstract

This study proposes the use of a novel nonlinear inerter-based device in vibration suppression of the ship propulsion shafting system and evaluates its performance. The device consists of an axial inerter and a pair of lateral inerters to create geometric nonlinearity. The system response subjected to propeller forces is determined by using the harmonic balance method with alternating-frequency-time technique and a numerical time-marching method. The force transmissibility and energy flow variables are employed to assess the performance of the device. The results show that the proposed device can reduce the peak force and energy transmission to the foundation while increase the energy dissipation within the device. Its use can lead to an improved vibration attenuation effect than the traditional mass-spring-damper device for low-frequency vibration. The configurations of the nonlinear inerter-based device can be adjusted to obtain an anti-peak at a resonance frequency of the original system, providing superior vibration suppression performance.

Keywords: Inerter; Vibration suppression; Propulsion shafting system; Longitudinal vibration; Power flow

1 Introduction

The propellers of ships and submarines can generate undesired fluctuating force in an unsteady non-uniform wake field caused by the protrusions of control surfaces or asymmetry of the hull (Zhu and Xie et al., 2021). The fluctuated thrust will be transmitted through the propulsion shafting system to the supporting foundation and excites the hull. It can result in structural vibrations and structure-borne noise, hence affecting crew comfort (Zhang et al., 2021). Moreover, such vibrations can lead to a high level of underwater acoustic radiation which is harmful to the ocean environment as well as the acoustic performance of vessels (Xie et al., 2021).

Some past research has shown that the axial component of the fluctuating force transmitted in a longitudinal direction along the shafting is the major vibration transmission path (Huang et al., 2018). To control the transmission of vibration, the use of active vibration suppression devices such as active vibration absorbers and magnetic actuators has been studied (Xie et al., 2021; Merz et al., 2013). The passive vibration suppression devices also attracted much research interest due to their advantages of simpler and reliable structure as well as not relying on external power. Among the past research, the so-called hydraulic resonance changer, which operates like a dynamic vibration absorber, has been extensively investigated (Dylejko et al., 2007; Zhang et al., 2012). Other designs such as anti-resonant vibration isolator (Liu and Li et al., 2017), periodically layered isolators (Song et al., 2014) and dynamic absorber with negative stiffness (Huang et al., 2018) were also proposed. Most of the relevant work assumed linearity of the passive devices. However, in the operation of the propulsion shafting, there is a limitation on the axial displacement of the system. Therefore, the stiffness of vibration suppression device cannot be set too low and the natural frequency of the integrated system is relatively high. Considering that the low-frequency components are dominant in the spectrum of the axial fluctuated thrust (Liu and Li et al., 2017), those linear devices may not be able to provide effective mitigation for the low or ultra-low frequency of vibration transmission (Mofidian and Bardaweel, 2018).

Much research has been reported on exploiting nonlinearities to enhance the low-frequency mitigation performance of systems such as vehicle suspension systems (Wang and Jing, 2019) and shock absorbers (Yan et al., 2018). However, there are very few works exploiting nonlinear passive devices or the novel inerter device for the suppression of longitudinal vibration of the ship shafting system (Zhao et al., 2020). The inerter is a recently proposed passive device having the property that its applied force F_b is proportional to the relative accelerations across its two terminals, i.e., $F_\mathrm{b} = b(\dot{V}_1 - \dot{V}_2)$, where b is the inertance and $\dot{V}_1$ and $\dot{V}_2$ are the terminal accelerations (Smith and Wang, 2004). Such device can be constructed based on rack-pinion flywheel, ball-screw mechanism or fluid following in an inertial track (Swift et al., 2013). Past studies have shown a good vibration suppression performance of linear inerter-based vibration suppression device for engineering structures (Li et al., 2016; Zhu and Yang et al., 2021). Recent studies have demonstrated that the nonlinear inerter-based mechanism can further improve the attenuation performance of vibration isolators (Wang et al., 2021; Yang et al., 2019) and a passive structural joint (Dong et al., 2021). It is of interest to employ a nonlinear vibration suppression device in the propulsion shafting system for a possible better reduction of longitudinal vibration transmission.

In the performance evaluation of the vibration suppression devices in the ship shafting system, the response amplitude and force transmissibility have usually been employed as indicators. The time-averaged vibration power flow combines the velocity, force and their relative phase angle in a single quantity, and hence can provide a more comprehensive quantification on the vibration transmission from the energy perspective (Goyder and White, 1980). The power flow indices have been widely accepted in the vibration transmission evaluation of linear systems (Xiong et al., 2003). Recent years have seen a development of power flow analysis (PFA) for the investigation of nonlinear systems (Dai et al., 2020, 2021), including nonlinear absorbers and nonlinear isolators (Yang et al., 2015, 2016).

In this research, a nonlinear tuned mass damper inerter (TMDI) created by a geometric nonlinearity is proposed and embedded in the longitudinal vibration transmission path of a typical propulsion shafting system. The effectiveness of the TMDI is assessed by the force transmissibility and time-averaged power flow variables. The effects of the parameters of inerters and the nonlinear configurations on the performance of TMDI are examined. The paper is organized as follows. In Section 2, the modelling of the ship shafting system with the TMDI is carried out. In Section 3, the dynamic analysis of the system and definitions of the performance indicators are presented. The influence of design parameters of the TMDI on the attenuation of longitudinal vibration transmission is investigated in Section 4, which is then followed by conclusions.

2 Modelling of the shafting system with the inerter-based device

Figure 1 outlines a generic propeller-shaft system with the shaft supported by the stern, intermediate and thrust bearings. The thrust bearing is connected to the foundation via the base structure. The main longitudinal vibration transmission path is along with the shaft through the thrust bearing and to the foundation structure, which can then excite the ship hull and generate undesired vibration and noise. The stern bearing and intermediate bearing only provide radial stiffness and damping, both bearings are not contributing to the longitudinal vibration transmission (Zou et al., 2019). To suppress the excessive vibration transmission, an TMDI is embedded in the thrust bearing base.

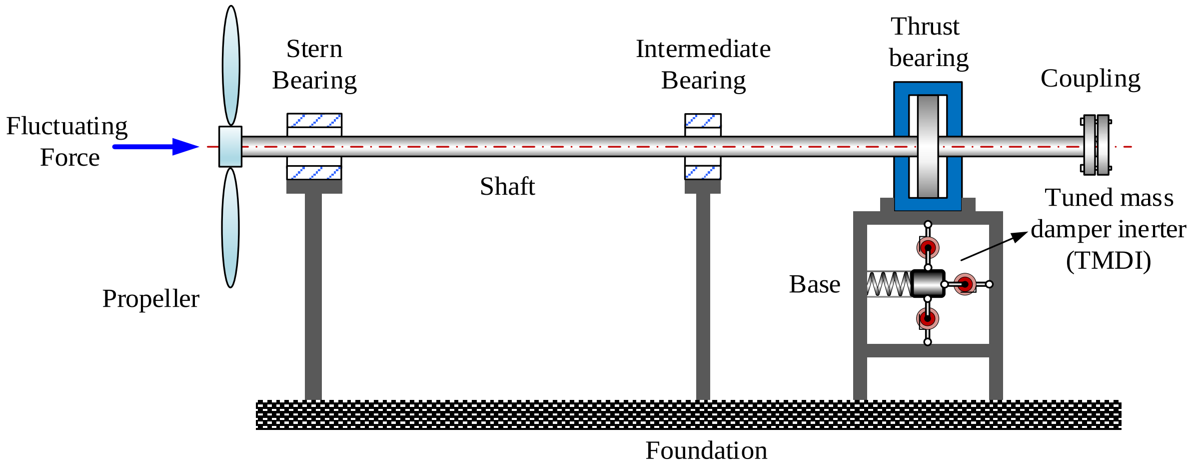

Figure. 1. Schematic representation of the propeller-shaft-bearing system considering an TMDI.

In accordance with the longitudinal vibration transmission path, the model of the ship shafting system can be simplified and presented as shown in Fig. 2(a). The fluctuating force applied on the propeller is assumed to be a harmonic excitation force $f_0 \exp(\mathrm{i}\omega t)$. The mass of the propeller is m_p. The shaft is a uniform beam with Young's modulus E, cross-sectional area a_s and length l_s. Here it is modelled as a massless elastic spring in the longitudinal vibration analysis (Liu and Lai et al., 2017). The equivalent stiffness k_s of the shaft can be calculated by $Ea_\mathrm{s}/l_\mathrm{s}$. The thrust bearing with mass m_t, stiffness k_t and damping c_t is installed on the bearing base of mass m_b. The bearing base is supported by the foundation with stiffness k_b and damping c_b. For comparison purposes, a tuned mass damper (TMD) comprising an elastic spring k_1, a viscous damper c_1 and a mass m_1 is mounted at terminal A within the frame of the bearing base, as shown in Fig. 2(a). The displacement responses of the propeller, the thrust bearing, the TMD mass and the base are represented by x_p, x_t x_1 and x_b, respectively. The parameter values of the shafting system are presented in Table 1. The scale of parameter is consistent with those in the past research (Dylejko et al., 2007; Merz et al., 2013; Huang et al., 2018), and the typical values are selected for demonstrating the use of TMDI.

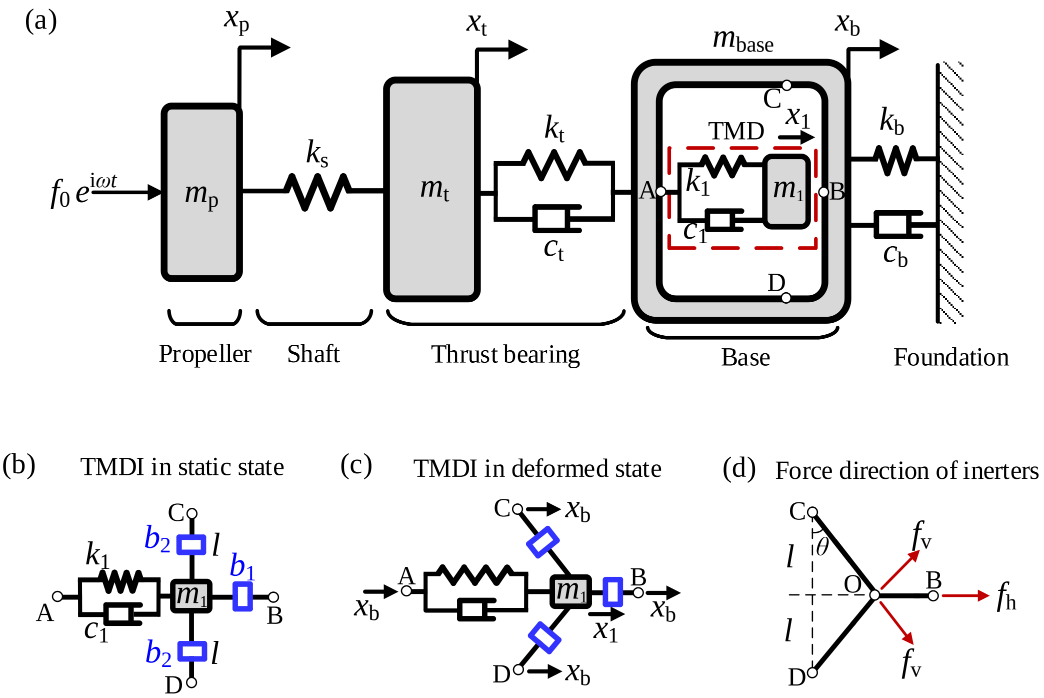

Figure. 2. Schematic of (a) the longitudinal vibration model of ship shafting system using the TMD, (b) the proposed TMDI in static-state and (c) the TMDI in deformed state.

Table 1. Parameters of the ship-shafting system

<table>
<tr><th>Name</th><th colspan="4">Physical parameters</th></tr>
<tr><td>Propeller</td><td colspan="2">Mass m_p:
1.5e4 kg</td><td colspan="2">Forcing amplitude:
10e5 kN</td></tr>
<tr><td>Shaft</td><td>Young's Modulus E:
200 GPa</td><td colspan="2">Cross-sectional area a_s:
0.7 m^2</td><td>Length l_s:
14 m</td></tr>
<tr><td>Thrust bearing</td><td>Mass m_t:
5e2 kg</td><td colspan="2">Stiffness k_t :
10e10 N/m</td><td>Damping c_t:
2.24e4 Ns/m</td></tr>
<tr><td>TMD</td><td>Mass m_1:
2.5e3 kg</td><td colspan="2">Stiffness k_1:
10e10 N/m</td><td>Damping c_1:
2.24e4 Ns/m</td></tr>
<tr><td>Bearing Base</td><td>Mass m_b:
5e3 kg</td><td>Stiffness k_b:
10e10 N/m</td><td>Length l:
1 m</td><td>Damping c_b:
1.12e3 Ns/m</td></tr>
</table>

As shown in Fig. 2(b), the proposed TMDI is attached to the bearing base at its left terminal A. Compared with the TMD, an axial inerter and a pair of lateral inerters are inserted to form the TMDI. The axial inerter with inertance of b_1 connects the mass m_1 to the bearing base at terminal B in the horizontal direction. The pair of lateral inerters with the same inertance of b_2 connects mass m_1 to the bearing base at terminals C and D, respectively. The static vertical distance between the mass m_1 and the upper or the lower base connection points C or D is set as l.

Figures 2(c) shows the system with relative displacement r between the base and the TMDI mass defined as $r = x_1 - x_\mathrm{b}$. Fig. 2(d) depicts the force directions of inerters. The angle between CO and CD is θ ($\sin\theta = r/\sqrt{l^2 + r^2}$). Noting that the terminal O is attached to mass m_1 and the terminals B, C and D are attached to base m_b, the force of the axial inerter f_h is the function of the relative acceleration $\ddot{r}$ between two masses as $f_\mathrm{h} = b_1\ddot{r}$. The relative velocity between point O and point C along the axis of the lateral inerter is $v = \dot{r}\sin\theta$. Then the inerter force f_v applied along the CO is obtained as

$$f_\mathrm{v} = b_2\frac{\mathrm{d}(v)}{\mathrm{d}t} = b_2\left(\ddot{r}\sin\theta + \frac{l^2\dot{r}^2}{(l^2+r^2)\sqrt{l^2+r^2}}\right). \quad (1)$$

According to the symmetricity of the TMDI, the total nonlinear inerter force applied on the mass m_1 is

$$f_\mathrm{tmdi}(r,\dot{r},\ddot{r},l,b_1,b_2) = f_\mathrm{h} + 2f_\mathrm{v}\sin\theta = b_1\ddot{r} + 2b_2\left(\frac{r^2\ddot{r}}{l^2+r^2} + \frac{l^2 r\dot{r}^2}{(l^2+r^2)^2}\right). \quad (2)$$

It shows that the nonlinear force depends on the relative displacement, velocity, and acceleration (Yang et al., 2019).

Based on the free body diagram of the mass m_1, the equation of motion is obtained:

$$m_1\ddot{x}_1 + k_1 r + c_1\dot{r} + f_\mathrm{tmdi}(r,\dot{r},\ddot{r},l,b_1,b_2) = 0. \quad (3)$$

The equations of motion of the system with the proposed TMDI are written in a matrix form as

$$\begin{bmatrix} m_\mathrm{p} & 0 & 0 & 0 \\ 0 & m_\mathrm{t} & 0 & 0 \\ 0 & 0 & m_1 & 0 \\ 0 & 0 & 0 & m_\mathrm{b} \end{bmatrix}\begin{Bmatrix} \ddot{x}_\mathrm{p} \\ \ddot{x}_\mathrm{t} \\ \ddot{x}_1 \\ \ddot{x}_\mathrm{b} \end{Bmatrix} + \begin{bmatrix} 0 & 0 & 0 & 0 \\ 0 & c_\mathrm{t} & 0 & -c_\mathrm{t} \\ 0 & 0 & c_1 & -c_1 \\ 0 & -c_\mathrm{t} & -c_1 & c_1 + c_\mathrm{t} + c_\mathrm{b} \end{bmatrix}\begin{Bmatrix} \dot{x}_\mathrm{p} \\ \dot{x}_\mathrm{t} \\ \dot{x}_1 \\ \dot{x}_\mathrm{b} \end{Bmatrix} +$$

$$\begin{bmatrix} k_\mathrm{s} & -k_\mathrm{s} & 0 & 0 \\ -k_\mathrm{s} & k_\mathrm{s} + k_\mathrm{t} & 0 & -k_\mathrm{t} \\ 0 & 0 & k_1 & -k_1 \\ 0 & -k_\mathrm{t} & -k_1 & k_1 + k_\mathrm{t} + k_\mathrm{b} \end{bmatrix}\begin{Bmatrix} x_\mathrm{p} \\ x_\mathrm{t} \\ x_1 \\ x_\mathrm{b} \end{Bmatrix} + \begin{Bmatrix} 0 \\ 0 \\ f_\mathrm{tmdi}(r,\dot{r},\ddot{r},l,b_1,b_2) \\ -f_\mathrm{tmdi}(r,\dot{r},\ddot{r},l,b_1,b_2) \end{Bmatrix} = \begin{Bmatrix} f_0\exp(\mathrm{i}\omega t) \\ 0 \\ 0 \\ 0 \end{Bmatrix}, \quad (4)$$

where $r = x_1 - x_\mathrm{b}$, $\dot{r} = \dot{x}_1 - \dot{x}_\mathrm{b}$, $\ddot{r} = \ddot{x}_1 - \ddot{x}_\mathrm{b}$. To facilitate later parametric study, the following variables and dimensionless parameters are introduced:

$$\omega_\mathrm{t} = \sqrt{\frac{k_\mathrm{t}}{m_\mathrm{t}}}, \zeta_\mathrm{t} = \frac{c_\mathrm{t}}{2m_\mathrm{t}\omega_\mathrm{t}}, \zeta_1 = \frac{c_1}{2m_\mathrm{t}\omega_\mathrm{t}}, \zeta_\mathrm{b} = \frac{c_\mathrm{b}}{2m_\mathrm{t}\omega_\mathrm{t}} X_\mathrm{p} = \frac{x_\mathrm{p}}{l}, X_\mathrm{t} = \frac{x_\mathrm{t}}{l}, X_1 = \frac{x_1}{l}, X_\mathrm{b} = \frac{x_\mathrm{b}}{l}, R = \frac{r}{l}, \mu_\mathrm{p} = \frac{m_\mathrm{p}}{m_\mathrm{t}},$$

$$\mu_1 = \frac{m_1}{m_\mathrm{t}}, \mu_\mathrm{b} = \frac{m_\mathrm{b}}{m_\mathrm{t}}, \lambda_1 = \frac{b_1}{m_\mathrm{t}}, \lambda_2 = \frac{b_2}{m_\mathrm{t}}, \kappa_\mathrm{s} = \frac{k_\mathrm{s}}{k_\mathrm{t}}, \kappa_1 = \frac{k_1}{k_\mathrm{t}}, \kappa_\mathrm{b} = \frac{k_\mathrm{b}}{k_\mathrm{t}}, F_0 = \frac{f_0}{lk_\mathrm{t}}, \Omega = \frac{\omega}{\omega_\mathrm{t}}, \tau = \omega_\mathrm{t} t, \quad (5a\text{-}5t)$$

where ω_t and ζ_t are the undamped natural frequency and damping ratio of the thrust bearing, respectively. ζ_1 and ζ_b are the damping ratios of the TMDI and foundation structure, respectively. X_p, X_t, X_1 and X_b are the dimensionless displacement responses, while R is the dimensionless relative displacement. μ_p, μ_1 and μ_b are mass ratios, λ_1 and λ_2 are the inertance to mass ratios of the axial and lateral inerter, respectively. κ_{s}, κ_1 and κ_{b} are the stiffness ratios. F_0 and Ω are the non-dimensional forcing amplitude and frequency of the harmonic fluctuation force applied on the propeller, respectively. τ is the dimensionless time. The non-dimensional equations of motion are then expressed as:

$$\begin{bmatrix} \mu_{\mathrm{p}} & 0 & 0 & 0 \\ 0 & 1 & 0 & 0 \\ 0 & 0 & \mu_1 & 0 \\ 0 & 0 & 0 & \mu_{\mathrm{b}} \end{bmatrix} \begin{Bmatrix} X_{\mathrm{p}}'' \\ X_{\mathrm{t}}'' \\ X_1'' \\ X_{\mathrm{b}}'' \end{Bmatrix} + \begin{bmatrix} 0 & 0 & 0 & 0 \\ 0 & 2\zeta_{\mathrm{t}} & 0 & -2\zeta_{\mathrm{t}} \\ 0 & 0 & 2\zeta_1 & -2\zeta_1 \\ 0 & -2\zeta_{\mathrm{t}} & -2\zeta_1 & 2(\zeta_1+\zeta_{\mathrm{b}}+\zeta_{\mathrm{t}}) \end{bmatrix} \begin{Bmatrix} X_{\mathrm{p}}' \\ X_{\mathrm{t}}' \\ X_1' \\ X_{\mathrm{b}}' \end{Bmatrix} +$$

$$\begin{bmatrix} \kappa_{\mathrm{s}} & -\kappa_{\mathrm{s}} & 0 & 0 \\ -\kappa_{\mathrm{s}} & \kappa_{\mathrm{s}}+1 & 0 & -1 \\ 0 & 0 & \kappa_1 & -\kappa_1 \\ 0 & -1 & -\kappa_1 & \kappa_1+\kappa_{\mathrm{b}}+1 \end{bmatrix} \begin{Bmatrix} X_{\mathrm{p}} \\ X_{\mathrm{t}} \\ X_1 \\ X_{\mathrm{b}} \end{Bmatrix} + \begin{Bmatrix} 0 \\ 0 \\ F_{\mathrm{TMDI}}(R,R',R'',\lambda_1,\lambda_2) \\ -F_{\mathrm{TMDI}}(R,R',R'',\lambda_1,\lambda_2) \end{Bmatrix} = \begin{Bmatrix} F_0 \exp(\mathrm{i}\Omega\tau) \\ 0 \\ 0 \\ 0 \end{Bmatrix}, \quad (6)$$

where

$$F_{\mathrm{TMDI}}(R,R',R'',\lambda_1,\lambda_2) = \lambda_1 R'' + 2\lambda_2\left(\frac{R^2R''}{1+R^2} + \frac{RR'^2}{(1+R^2)^2}\right). \quad (7)$$

3 Dynamics and performance indicators of vibration suppression

3.1 Response analysis of the system

To evaluate the performance of the proposed TMDI, the governing equations of the ship shafting system in Eq. (6) need to be solved first. In this study, the semi-analytical harmonic balance method with alternating-frequency-time technique (HB-AFT) is employed (Von Groll and Ewins, 2001). A numerical time-marching method (i.e., adaptive Runge-Kutta method) is also used for comparison. In the HB-AFT scheme, the corresponding steady-state responses of each mass are firstly approximated by a N-th order Fourier series expressed as

$$X_{\mathrm{p}} = \sum_{n=0}^{N} \tilde{Z}_{(\mathrm{p},n)} \exp(\mathrm{i}n\Omega\tau), \qquad X_{\mathrm{t}} = \sum_{n=0}^{N} \tilde{Z}_{(\mathrm{t},n)} \exp(\mathrm{i}n\Omega\tau), \quad (8a, 8b)$$

$$X_1 = \sum_{n=0}^{N} \tilde{Z}_{(1,n)} \exp(\mathrm{i}n\Omega\tau), \qquad X_{\mathrm{b}} = \sum_{n=0}^{N} \tilde{Z}_{(\mathrm{b},n)} \exp(\mathrm{i}n\Omega\tau), \quad (8c, 8d)$$

where $1 \le n \le N$, $\tilde{Z}_{(n)}$ is the complex Fourier coefficients for the n-th order approximation. The nonlinear inertance force generated by the proposed TMDI can be approximated by

$$F_{\mathrm{TMDI}} = \sum_{n=0}^{N} \widetilde{H}_n \exp(\mathrm{i}n\Omega\tau), \quad (9)$$

where F_{TMDI} has been defined by Eq. (7) and $\widetilde{H}_n$ is the n-th complex Fourier coefficients. To determine $\widetilde{H}_n$, the AFT scheme is applied here by substituting displacement, velocity and acceleration responses (obtained from the differentiation of Eq. (8)) into Eq. (9). Then the time history of the nonlinear force $F_{\mathrm{TMDI}}(\tau)$ can be obtained and Fourier transformed to find the coefficient $\widetilde{H}_n$.

The Fourier approximations of responses expressed in Eq. (8) and nonlinear force generated by the inerters in Eq. (9) can be substituted into the dimensionless governing equation Eq. (6). The HB method is then used by balancing the complex coefficients of the corresponding harmonics with the same order. The n-th order harmonic balanced equation is expressed as

$$\left(-(n\Omega)^2\begin{bmatrix}\mu_\mathrm{p} & 0 & 0 & 0\\ 0 & 1 & 0 & 0\\ 0 & 0 & \mu_1 & 0\\ 0 & 0 & 0 & \mu_\mathrm{b}\end{bmatrix}+\mathrm{i}(n\Omega)\begin{bmatrix}0 & 0 & 0 & 0\\ 0 & 2\zeta_\mathrm{t} & 0 & -2\zeta_\mathrm{t}\\ 0 & 0 & 2\zeta_1 & -2\zeta_1\\ 0 & -2\zeta_\mathrm{t} & -2\zeta_1 & 2(\zeta_1+\zeta_\mathrm{b}+\zeta_\mathrm{t})\end{bmatrix}+\right.$$

$$\left.\begin{bmatrix}\kappa_\mathrm{s} & -\kappa_\mathrm{s} & 0 & 0\\ -\kappa_\mathrm{s} & \kappa_\mathrm{s}+1 & 0 & -1\\ 0 & 0 & \kappa_1 & -\kappa_1\\ 0 & -1 & -\kappa_1 & \kappa_1+\kappa_\mathrm{b}+1\end{bmatrix}\right)\begin{Bmatrix}\tilde{Z}_{(\mathrm{p},n)}\\ \tilde{Z}_{(\mathrm{t},n)}\\ \tilde{Z}_{(1,n)}\\ \tilde{Z}_{(\mathrm{b},n)}\end{Bmatrix}=\begin{Bmatrix}F_0\\ 0\\ 0\\ 0\end{Bmatrix}+\begin{Bmatrix}0\\ 0\\ -\tilde{H}_n\\ \tilde{H}_n\end{Bmatrix}. \quad (10)$$

Recalling the range of order n is $1 \le n \le N$, a number of $4(2N+1)$ algebraic equations are obtained, which are then solved by the Newton-Rapson method. Noting that a higher order N of the HB method can provide a more accurate approximation to the nonlinear force as well as the steady-state response of the system, but will significantly increase the computational burden. To strike a balance of accuracy and efficiency, the HB order N in this research is set as 7 based on the convergence study. In the meantime, to trace the solution branches, the pseudo-arclength continuation method is applied together with HB to determine the responses (Seydel, 2010).

For the special case of TMDI system without the lateral inerters (with $\lambda_2 = 0$), the governing equation can be directly solved. By substituting Eq. (8) with $N = 1$ into Eq. (6), the equation of motion can then be written as

$$\begin{bmatrix}-\Omega^2\mu_\mathrm{p}+\kappa_\mathrm{s} & -\kappa_\mathrm{s} & 0 & 0\\ -\kappa_\mathrm{s} & A & 0 & -2\mathrm{i}\Omega\zeta_\mathrm{t}-1\\ 0 & 0 & B & -\kappa_1-2\mathrm{i}\Omega\zeta_1+\lambda_1\Omega^2\\ 0 & -2\mathrm{i}\Omega\zeta_\mathrm{t}-1 & -\kappa_1-2\mathrm{i}\Omega\zeta_1+\lambda_1\Omega^2 & C\end{bmatrix}\begin{Bmatrix}\tilde{Z}_{(\mathrm{p},1)}\\ \tilde{Z}_{(\mathrm{t},1)}\\ \tilde{Z}_{(1,1)}\\ \tilde{Z}_{(\mathrm{b},1)}\end{Bmatrix}=\begin{Bmatrix}F_0\\ 0\\ 0\\ 0\end{Bmatrix}, \quad (11)$$

where $A = -\Omega^2 + \kappa_\mathrm{s} + 2\mathrm{i}\Omega\zeta_\mathrm{t} + 1$, $B = -\Omega^2(\mu_1 + \lambda_1) + 2\mathrm{i}\Omega\zeta_1 + \kappa_1$ and $C = \kappa_1 + \kappa_\mathrm{b} + 2\mathrm{i}\Omega(\zeta_1 + \zeta_\mathrm{b} + \zeta_\mathrm{t}) - \Omega^2(\mu_\mathrm{b} + \lambda_1) + 1$. Then the complex coefficients of the response $\tilde{Z}_{(\mathrm{p},1)}$, $\tilde{Z}_{(\mathrm{t},1)}$, $\tilde{Z}_{(1,1)}$ and $\tilde{Z}_{(\mathrm{b},1)}$ can be determined following standard matrix operations.

3.2 Force transmissibility and energy indices

To evaluate the effectiveness of the TMDI on the suppression of vibration transmission to the foundation, the force transmission, kinetic energy, and power indices including the time-averaged input, dissipated and transmitted power are selected as performance indicators. The force transmissibility TR to the foundation is defined as

$$TR = \frac{|F_\mathrm{T}|_\mathrm{max}}{F_0}, \quad (12)$$

where F_T is the transmitted force to the foundation with $F_\mathrm{T} = \kappa_\mathrm{b} X_\mathrm{b} + 2\zeta_\mathrm{b} X_\mathrm{b}'$.

The maximum kinetic energy of the bearing base E_b can be used to assess the vibration level of the bearing base and also the performance of the TMDI, which is defined as

$$E_\mathrm{b} = \frac{1}{2}\{(X_\mathrm{b}')_\mathrm{max}\}^2. \quad (13)$$

The time-averaged input power $\overline{P}_{\mathrm{in}}$ into the shafting system during the time span of $[\tau_0, \tau_0 + \tau_{\mathrm{p}}]$ is obtained by

$$\overline{P}_{\mathrm{in}} = \frac{1}{\tau_{\mathrm{p}}} \int_{\tau_0}^{\tau_0+\tau_{\mathrm{p}}} P_{\mathrm{in}} \, \mathrm{d}\tau = \frac{1}{\tau_{\mathrm{p}}} \Re \int_{\tau_0}^{\tau_0+\tau_{\mathrm{p}}} \{F_0 \mathrm{e}^{\mathrm{i}\Omega\tau}\} \Re\{X_{\mathrm{p}}'\} \, \mathrm{d}\tau = \frac{1}{2} F_0 \Re\left\{\left(\mathrm{i}\Omega \tilde{Z}_{(\mathrm{p},1)}\right)^*\right\}, \tag{14}$$

where τ_{p} is set as one period of harmonic cycle in steady state as $\tau_{\mathrm{p}} = 2\pi/\Omega$. $\Re\{\}$ and $()^*$ denote the operations of taking real part and complex conjugate of the variable in the bracket, respectively. Note that smaller possible values of kinetic energy E_{b} and time-averaged input power $\overline{P}_{\mathrm{in}}$ are desirable in the suppression of longitudinal vibration transmission.

The time-averaged power dissipation $\overline{P}_{\mathrm{d1}}$ of the damper c_1 is also employed to evaluate the energy absorption performance of the TMDI. A larger amount of energy dissipation $\overline{P}_{\mathrm{d1}}$ in TMDI suggests less vibrational energy transmitted to the ship hull. It is defined as

$$\overline{P}_{\mathrm{d1}} = \frac{1}{\tau_{\mathrm{p}}} \int_{\tau_0}^{\tau_0+\tau_{\mathrm{p}}} 2\zeta_1 \left\{\Re\{X_1' - X_{\mathrm{b}}'\}\right\}^2 \mathrm{d}\tau = \frac{1}{2} \Re\left\{\left[\sum_{n=0}^{N} \mathrm{i}n\Omega(\tilde{Z}_{(1,n)} - \tilde{Z}_{(\mathrm{b},n)})\right]^* \left[2\zeta_1 \sum_{n=0}^{N} \mathrm{i}n\Omega(\tilde{Z}_{(1,n)} - \tilde{Z}_{(\mathrm{b},n)})\right]\right\} = \zeta_1 \left|\sum_{n=0}^{N} \mathrm{i}n\Omega\left(\tilde{Z}_{(1,n)} - \tilde{Z}_{(\mathrm{b},n)}\right)\right|^2. \tag{15}$$

According to the energy conservation law, the time-averaged vibrational power transmission to the foundation is obtained as:

$$\overline{P}_{\mathrm{t}} = \frac{1}{\tau_{\mathrm{p}}} \int_{\tau_0}^{\tau_0+\tau_{\mathrm{p}}} P_{\mathrm{t}} \, \mathrm{d}\tau = \frac{1}{\tau_{\mathrm{p}}} \int_{\tau_0}^{\tau_0+\tau_{\mathrm{p}}} 2\zeta_{\mathrm{b}} \left\{\Re\{X_{\mathrm{b}}'\}\right\}^2 \mathrm{d}\tau = \frac{1}{2} \Re\left\{\left[\sum_{n=0}^{N} \mathrm{i}n\Omega(\tilde{Z}_{(\mathrm{b},n)})\right]^* \left[2\zeta_{\mathrm{b}} \sum_{n=0}^{N} \mathrm{i}n\Omega(\tilde{Z}_{(\mathrm{b},n)})\right]\right\} = \zeta_{\mathrm{b}} \left|\sum_{n=0}^{N} \mathrm{i}n\Omega\left(\tilde{Z}_{(\mathrm{b},n)}\right)\right|^2. \tag{16}$$

4 Results and discussion

In this part, the effectiveness of the proposed TMDI for the suppression of the longitudinal vibration transmission of the ship shafting is evaluated using the afore-defined performance indicators. The effects of the inertance of the axial inerter and the pair lateral inerters are investigated. The values of the physical parameters have been provided in Table 1. The dimensionless system parameters are obtained as $u_{\mathrm{p}} = 30$, $u_{\mathrm{b}} = 10$, $u_1 = 5$. $\kappa_{\mathrm{s}} = \kappa_1 = \kappa_{\mathrm{b}} = \kappa_{\mathrm{t}} = 1$, $\zeta_{\mathrm{t}} = \zeta_1 = 0.01$, $\zeta_{\mathrm{b}} = 0.005$ and $F_0 = 0.01$.

The effectiveness of the TMDI without using the lateral inerters ($\lambda_2 = 0$) is firstly examined. Figs. 3 and 4 present the variations of the performance indicators against the excitation frequency. The results are obtained by HB method and validated by the adaptive Runge-Kutta (RK) method. Three different cases are selected with the inertance-to-mass ratio λ_1 changing from 0 to 2 and to 10, denoted by solid lines. Note that the case with $\lambda_1 = 0$ corresponds to the system using TMD without inerters, as shown in Fig. 2(a). Moreover, a reference case denoting the system without TMD is considered with the results marked by a dashed line for comparison.

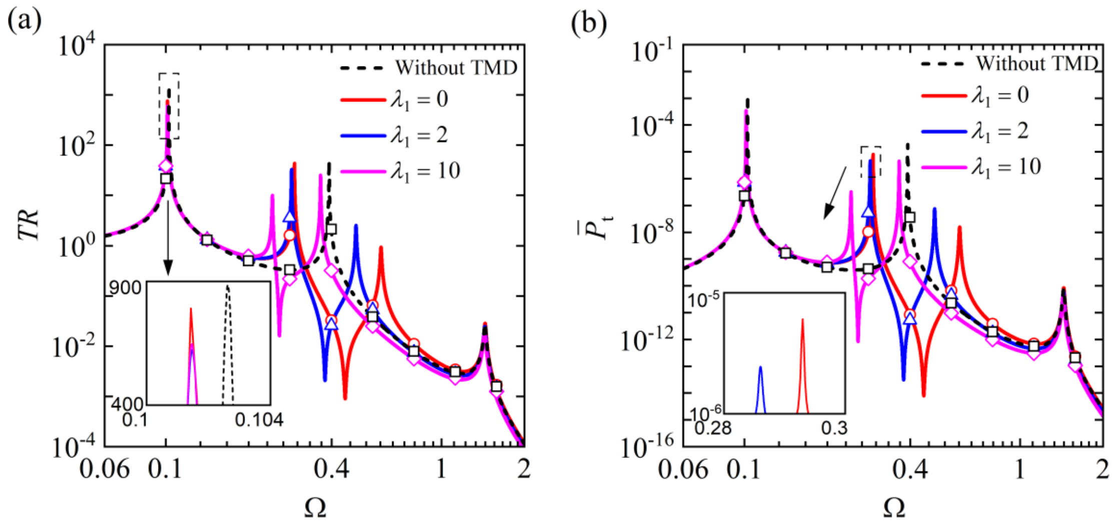

Figure. 3. Effect of the TMDI with different configurations on the (a) force transmissibility TR and (b) transmitted power $\bar{P}_t$. The dashed line represents the original system without TMD. The red line denotes the system employing a TMD ($\lambda_1 = 0$). The blue and pink lines mark the system using the TMDI with $\lambda_1 = 2$ and 10, respectively. Symbols: RK results

Figures 3(a) and (b) show the force transmissibility TR to the foundation and the time-averaged transmitted power $\bar{P}_t$ to the foundation, respectively. Comparing to the original system shown by the dashed curve, the addition of the TMD will introduce an additional DOF such that there is another resonance peak in each curve of TR or $\bar{P}_t$. It is demonstrated that the first peak of the TR and $\bar{P}_t$ near $\Omega = 0.1$ is slightly decreased by using TMD. By conducting modal analysis on the system in the case with $\lambda_2 = 2$, it is shown that the TMD mass and the base mass are moving in the out-of-phase mode at the frequency of $\Omega \approx 0.39$ while two masses are moving nearly in-phase at the frequency of $\Omega \approx 1.44$. As a result, the TMD will largely influence the response and the vibration transmission indices at the second original peak frequency of $\Omega \approx 0.39$ while shows little effect at the third original peak frequency of $\Omega \approx 1.44$. Since the dominant frequency of the external excitation on the propeller is usually low, the TMDI with a non-zero value of the inertance-to-mass ratio λ_1 exhibits a better vibration suppression performance than the TMD by shifting two peaks and the anti-peak of TR or $\bar{P}_t$ near $\Omega = 0.4$ to the low-frequency range. As the value of λ_1 increases, the second peak of both TR and $\bar{P}_t$ becomes smaller and the corresponding frequency is further reduced, which will benefit the attenuation of low-frequency vibration transmission to the foundation. Combining the TR and $\bar{P}_t$ curves, it is interesting to see the frequency of the anti-peak in the TMDI case with $\lambda_1 = 2$ is $\Omega \approx 0.38$, matching approximately with the second peak frequency of the original system without TMD. This phenomenon indicates that the property of the axial inerter can be tuned to achieve a desirable effective vibration suppression band without the need to trade off the spring stiffness of the TMDI. The resonance behaviour of the coupled system can be modified by adjusting inertance and the excessive vibration transmission in the original system can then be substantially attenuated.

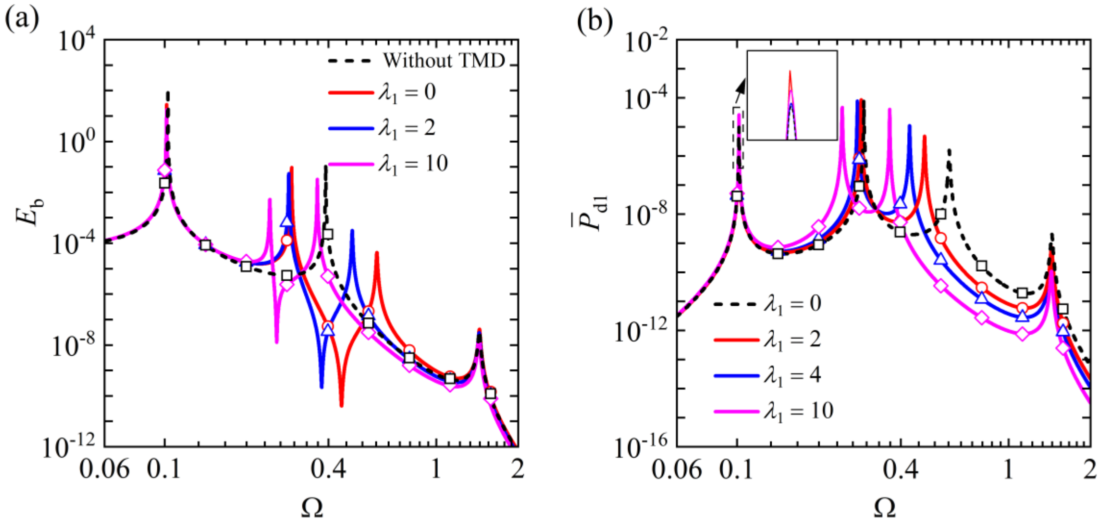

Figure. 4. Effect of the TMDI with different configurations on the (a) kinetic energy E_b and (b) dissipated power $\bar{P}_{d1}$. The dashed line represents the original system without TMD. In (a), the red line denotes the system employing a TMD ($\lambda_1 = 0$). The blue and pink lines mark the system using the TMDI with $\lambda_1 = 2$ and 10, respectively. In (b), the red, blue and pink lines mark the system using the TMDI with $\lambda_1 = 2$, 4 and 10, respectively. Symbols: RK results

Figure 4(a) shows the effects of TMDI on the maximum kinetic energy E_b of the bearing base. As a comparison to the referenced original system case without TMD, it is found that the TMD can lower the first peak of the kinetic energy. The second original peak of the reference case (dashed line) is split into two individual peaks with smaller values. With the proposed TMDI employing axial inerter ($\lambda_1 \neq 0$), the second and third peaks move to the left comparing to the TMD case ($\lambda_1 = 0$). In addition, the second peak value is further reduced, showing a good vibration suppression performance of the TMDI at low frequencies. In Fig. 4(b), three cases considering TMDI are presented with λ_1 changing from 2 to 4 and to 10. Comparing to the TMD ($\lambda_1 = 0$) case, the use of axial inerter can increase the amount of energy that is dissipated by the viscous damper of the TMDI in the frequency band between $0.1 < \Omega < 0.4$, away from peaks. Moreover, the addition of the axial inerter with a larger inertance λ_1 can increase substantially the first and third peak value of $\bar{P}_{d1}$. Those phenomena indicate that the proposed TMDI with the use of axial inerter can assist the reduction of longitudinal vibration by providing a stronger energy dissipation effect at low frequencies.

In Figs. 5 and 6, the effectiveness of the TMDI with both the axial and lateral inerters is investigated. The results are obtained by the combined use of the semi-analytical HB-AFT method and numerical continuation method. The adaptive Runge-Kutta (RK) method is also employed for comparison. The stability of the system is determined by the Floquet theory and confirmed by the RK method. The unstable range of the system is marked by dash-dotted line, as shown in the zoom-in subfigure in Figs. 5 and 6. Three different cases are selected with the lateral inertance-to-mass ratio λ_2 varying from 0 to 50, to 75, and to 100, while the axial inertance-to-mass ratio λ_1 is fixed as 1. A reference original system case without using TMDI is shown by a dashed curve for comparison.

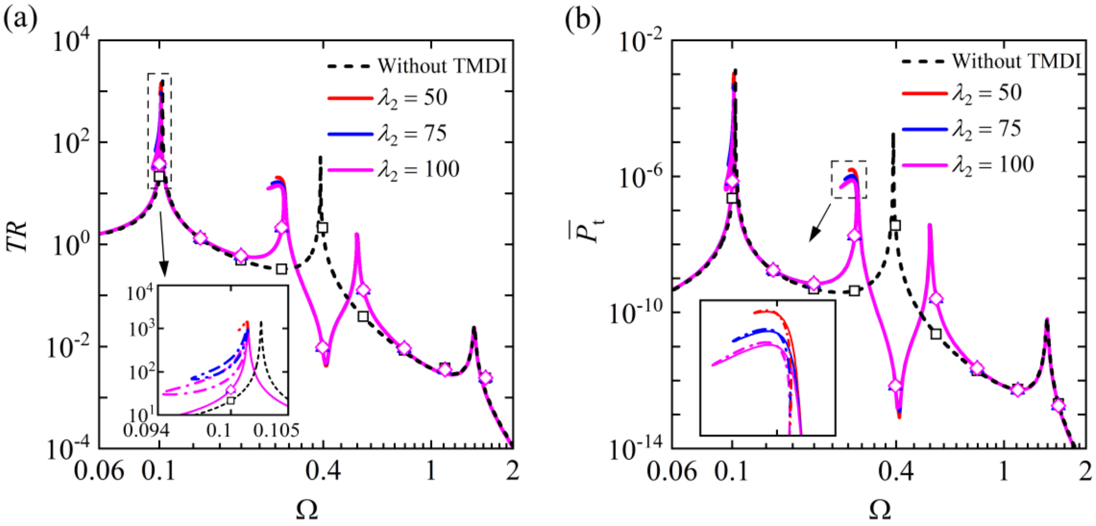

Figure. 5. Effect of TMDI with different configurations on the (a) force transmissibility TR and (b) transmitted power $\bar{P}_t$. The dashed line represents the original system without TMDI. The red, blue and pink lines mark the system using the TMDI with λ_2 =50, 75 and 100, respectively. Symbols: RK results

Figures 5(a), 5(b), 6(a) and 6(b) present the force transmissibility TR to the bearing base, the steady-state time-averaged energy transmission to the foundation $\bar{P}_t$, the time-averaged input power $\bar{P}_{in}$ and the maximum kinetic energy E_b of the bearing base, respectively. Comparing to the reference case of the original system. There is a slight left-movement of the first peak in each curve of Figs. 5 and 6 by the use of the TMDI. The first three peaks in the force transmissibility, power dissipation, kinetic energy and input power curves are extended to the left with lower peak values, demonstrating an enhanced suppression performance for low-frequency vibration transmission. With the increase of the lateral inertance λ_2 from 50 to 100, the first three peaks in each curve of those indices bend further to the low frequencies and the peak values become smaller. However, there is little change in corresponding peak frequencies of those performance indicators regardless of the variations of the lateral inertance λ_2. This is of contrast to the effect of the axial inerter, the addition of which can change substantially the peak frequency of those indices, as shown in Figs. 3 and 4.

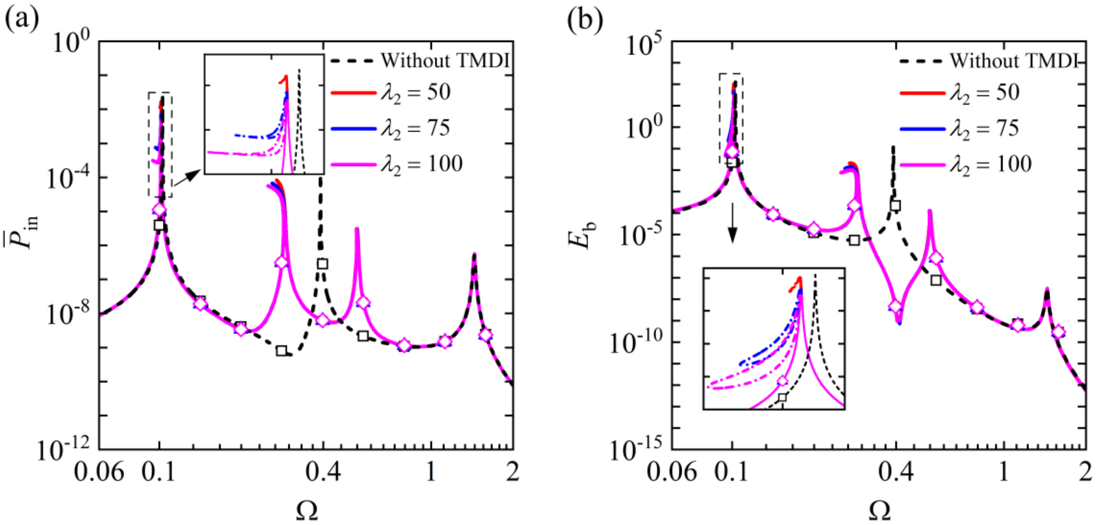

Figure. 6. Effect of TMDI with different configurations on the (a) input power $\bar{P}_{\text{in}}$ and (b) kinetic energy E_{b}. The dashed line represents the original system without TMDI. The red, blue and pink lines mark the system using the TMDI with the λ_2 =50, 75 and 100, respectively. Symbols: RK results

The main reason for the major differences in the effects of the axial and the lateral inerters is that the lateral inerters only take the effect when there is relatively large deformation in the geometry of the TMDI, i.e., a relatively large axial relative displacement between the TMDI mass m_1 and the bearing base m_{b}. When the frequency of the fluctuating force on the propeller is away from the resonant frequencies, the deformation of the TMDI is small and the nonlinear force term generated by the geometric nonlinearity of the lateral inerters will be small, leading to an insignificant contribution to the vibration transmission of the system. However, near the resonance, the lateral inerters can suppress considerably the system response and vibration transmission. Figs. 7(a) and (b) further demonstrates the effects of different inertance combinations of TMDI on the power input and power transmission, respectively. Four cases with different values of λ_1 and λ_2 are compared. The other parameters are set the same to the system in Figure 6. It can be summarized that the inertance of axial and lateral inerters can be carefully selected to tailor the characteristic of the device, providing a good vibration suppression performance at targeted frequency band.

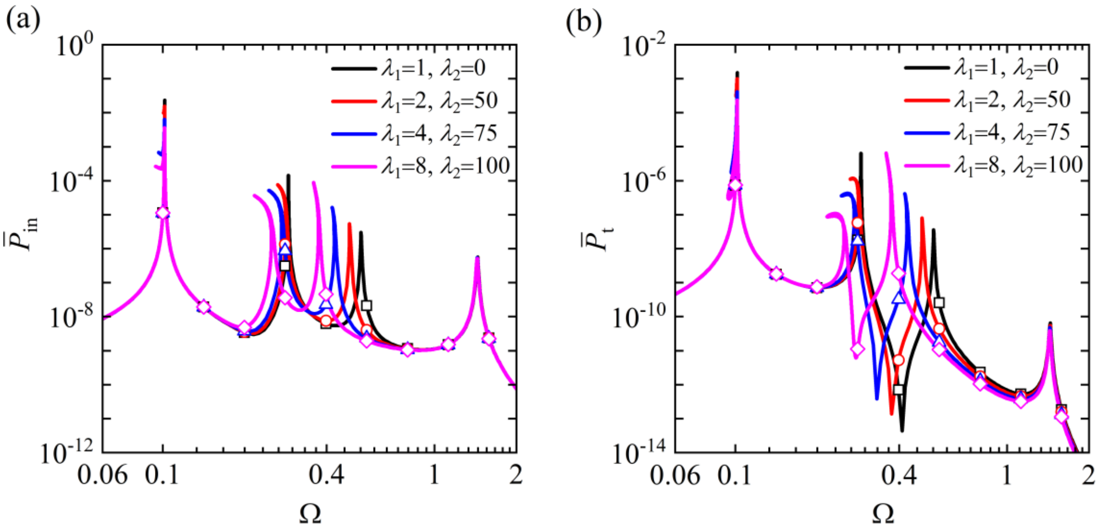

Figure. 7. Effect of TMDI with different inertance combinations on the (a) input power $\bar{P}_{\text{in}}$ and (b) power transmission $\bar{P}_{\text{t}}$. The black, red, blue and pink lines mark the system using the TMDI with the $\lambda_1 = 1$, $\lambda_2 = 0$; $\lambda_1 = 2$, $\lambda_2 = 50$; $\lambda_1 = 4$, $\lambda_2 = 75$; $\lambda_1 = 8$, $\lambda_2 = 100$, respectively. Symbols: RK results.

Figure 8 depicts the time histories of the vibration transmission indicators in the steady state at the first resonant frequency of the original system without TMDI ($\Omega = 0.1026$) in Figs. 8(a), (b) and (c), and at the second resonant frequency of the original system ($\Omega = 0.39$) in Figs. 8(d), (e) and (f). The red line and blue line mark the case with TMDI ($\lambda_1 = 1$, $\lambda_2 = 50$) and the case without TMDI, respectively. The results demonstrate that the use of TMDI can largely reduce the amplitude of the instantaneous power input, transmitted force and instantaneous power transmission to the foundation at original peak frequencies. Moreover, from Figs. 8(a), (c), (d) and (f), it is found that the proposed TMDI can reduce substantially the positive part of the instantaneous power input and power transmission at the first original peak frequency, leading to a much smaller amount of energy input into the system as well as less vibrational energy transmitted to the foundation.

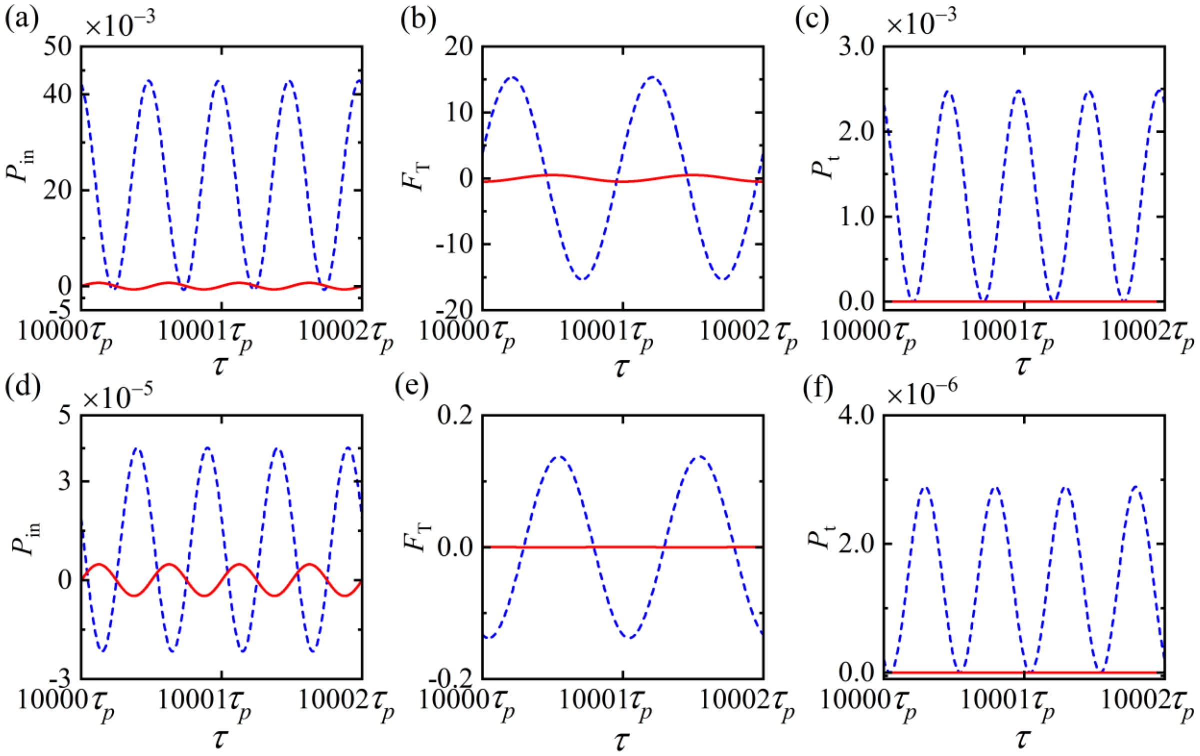

Figure. 8. Time histories of instantaneous vibration transmission indices at the first original resonant peak frequency of $\Omega = 0.1026$ in (a-c), and the second original resonant peak frequency of $\Omega = 0.39$ in (d-f). In (a) and (d): the input power P_{in}; in (b) and (e): the transmitted force F_T, in (b) and (e): the transmitted power P_t. The red and blue lines denote the cases with TMDI and without TMDI, respectively.

5 Conclusions

This study proposed the use of a nonlinear inerter-based vibration suppression device for enhanced attenuation of the longitudinal vibration transmission in the ship propulsion shafting system. The nonlinear device comprises a mass-spring-damper system, an axial inerter and a pair of lateral inerters creating geometric nonlinearity. The force transmissibility and power flow variables were employed to assess the performance of the device under variations of design parameters and configurations. It was found that the use of axial inerters can lower the peak force and power transmission from the bearing supporting base to the foundation. The resonant peaks in the kinetic energy, force transmission and power transmission curves were shifted to the low-frequency range. The lateral inerters can bend the main resonant peaks in the curves of force transmissibility, power input, power transmission and kinetic energy to the low frequencies with lower peak heights. The inertance of inerters can be adjusted to provide an anti-resonant frequency band so as to significantly attenuate the vibration transmission. With a comparison to the traditional mass-spring-damper device, the use of the proposed nonlinear inerter-based device demonstrates enhanced vibration mitigation performance, particularly for the low-frequency components of vibration transmission in the propulsion shafting system.

Acknowledgements

This work was supported by National Natural Science Foundation of China [Grant number 12172185, 51839005].

References

Dai W, Yang J and Shi B (2020) Vibration transmission and power flow in impact oscillators with linear and nonlinear constraints. *International Journal of Mechanical Sciences* 168: 105234.

Dai W and Yang J (2021) Vibration transmission and energy flow of impact oscillators with nonlinear motion constraints created by diamond-shaped linkage mechanism. *International Journal of Mechanical Sciences* 194: 106212.

Dong Z, Shi B, Yang J, et al. (2021) Suppression of vibration transmission in coupled systems with an inerter-based nonlinear joint. *Nonlinear Dynamics*. Epub ahead of print 16 September 2021. DOI: 10.1007/s11071-021-06847-9.

Dylejko PG, Kessissoglou NJ, Tso Y, et al. (2007) Optimisation of a resonance changer to minimise the vibration transmission in marine vessels. *Journal of Sound and Vibration* 300: 101-116.

Goyder HGD and White RG (1980) Vibrational power flow from machines into built-up structures, part I: Introduction and approximate analyses of beam and plate-like foundations. *Journal of Sound and Vibration* 68: 59-75.

Huang X, Su Z and Hua H (2018) Application of a dynamic vibration absorber with negative stiffness for control of a marine shafting system. *Ocean Engineering* 155: 131-143.

Liu JL, Lai GJ and Zeng FM (2017) Parameter optimization method for longitudinal vibration absorber of ship shaft system. *Chinese Journal of Ship Research* 12(3): 105-110.

Liu N, Li C, Yin C, et al. (2017) Application of a dynamic antiresonant vibration isolator to minimize the vibration transmission in underwater vehicles. *Journal of Vibration and Control* 24(17): 3819-3829.

Li Y, Jiang JZ and Neild S (2016) Inerter-based configurations for main-landing-gear shimmy suppression. *Journal of Aircraft* 54(2): 684-693.

Merz S, Kessissoglou N, Kinns R, et al. (2013) Passive and active control of the radiated sound power from a submarine excited by propeller forces. *Journal of Ship Research* 57: 59-71.

Mofidian SMM. and Bardaweel H. (2018). Displacement transmissibility evaluation of vibration isolation system employing nonlinear-damping and nonlinear-stiffness elements. *Journal of Vibration and Control* 24(18): 4247-4259.

Seydel R (2010) *Practical bifurcation and stability analysis*. New York: Springer;

Smith MC and Wang F-C (2004) Performance benefits in passive vehicle suspensions employing inerters. *Vehicle System Dynamics* 42: 235-257.

Song Y, Wen J, Yu D, et al. (2014) Reduction of vibration and noise radiation of an underwater vehicle due to propeller forces using periodically layered isolators. *Journal of Sound and Vibration* 333: 3031-3043.

Swift SJ, Smith MC, Glover AR, et al. (2013) Design and modelling of a fluid inerter. *International Journal of Control* 86: 2035-2051.

Von Groll G and Ewins DJ (2001) The harmonic balance method with arc-length continuation in rotor/stator contact problems. *Journal of Sound and Vibration* 241: 223-233.

Wang Y and Jing XJ (2019) Nonlinear stiffness and dynamical response characteristics of an asymmetric X-shaped structure. *Mechanical Systems and Signal Processing* 125: 142-169.

Wang Y, Li HX., Cheng C, et al. (2021) A nonlinear stiffness and nonlinear inertial vibration isolator. *Journal of Vibration and Control* 27(11-12): 1336-1352.

Xie X, Ren M, Zheng H, et al. (2021) Active vibration control of a time-varying shafting system using an adaptive algorithm with online auxiliary filter estimation. *Journal of Sound and Vibration* 513: 116430.

Xiong YP, Xing JT, Price WG. (2003) A general linear mathematical model of power flow analysis and control for integrated structure–control systems. *Journal of Sound and Vibration* 267: 301-334.

Yan L, Xuan S and Gong X (2018) Shock isolation performance of a geometric anti-spring isolator. *Journal of Sound and Vibration* 413: 120-143.

Yang J, Jiang JZ and Neild SA (2019) Dynamic analysis and performance evaluation of nonlinear inerter-based vibration isolators. *Nonlinear Dynamics* 99: 1823-1839.

Yang J, Xiong YP and Xing JT (2016) Vibration power flow and force transmission behaviour of a nonlinear isolator mounted on a nonlinear base. *International Journal of Mechanical Sciences* 115-116: 238-252.

Yang J, Xiong YP and Xing JT (2015) Power flow behaviour and dynamic performance of a nonlinear vibration absorber coupled to a nonlinear oscillator. *Nonlinear Dynamics* 80: 1063-1079.

Zhang Y, Xu W, Li Z, et al. (2021) Design and dynamic analysis of low-frequency mounting system for marine thrust bearing. *Journal of the Brazilian Society of Mechanical Sciences and Engineering* 43: 109.

Zhang Z, Rustighi E, Chen Y, et al. (2012) Active control of the longitudinal-lateral vibration of a shaft-plate coupled system. *Journal of Vibration and Acoustics* 134(6): 061002.

Zhao H, Yang Z, Ta N, et al. (2020) Longitudinal vibration reduction of ship propulsion shafting based on quasi-zero-stiffness isolator. *Journal of Vibration and Shock* 39: 90-95.

Zhu C, Yang J and Rudd C (2021) Vibration transmission and power flow of laminated composite plates with inerter-based suppression configurations. *International Journal of Mechanical Sciences* 190: 106012.

Zhu Y, Xie X. and Zhang Z. (2021). Investigation on vibration transmission control of a shafting system with active orthogonal support. *Journal of Vibration and Control*. Epub ahead of print 16 February 2021. DOI: 10.1177/1077546321993583.

Zou D, Jiao C, Ta N, et al. (2019) Theoretical study on the axial excitation force transmission characteristics of marine propellers. *Ocean Engineering* 189: 106364.